

A new methodological approach to assess the stability of discontinuous rocky cliffs using in-situ surveys supported by UAV-based techniques and 3-D finite element model: a case study

Fazio N.L.^{1a} *

n.fazio@ba.irpi.cnr.it

Perrotti M.^{1a}

Andriani G.F.^{2b}

Mancini F.^{3c}

Rossi P.^{3c}

Castagnetti C.^{3c}

Lollino P.^{1a}

^{1a}CNR - IRPI, Istituto di Ricerca Protezione Idrogeologica, Bari, Italy

^{2b}DISTEGEO, Dipartimento di Scienze della Terra e Geoambientali, Università degli Studi di Bari "Aldo Moro", Italy

^{3c}DIEF, Dipartimento di Ingegneria "Enzo Ferrari", Università degli Studi di Modena e Reggio Emilia, Italy

*Corresponding author.

ABSTRACT

This paper aims to present a new methodological approach for the stability assessment of coastal cliffs constituted of discontinuous rock masses. The method entails in situ specific geostructural and geomechanical surveys, three-dimensional UAV-based Photogrammetric structural models, laboratory geotechnical tests and, two- and three-dimensional finite element analysis (FEM). The application of the method to a case study is then presented and discussed; it regards a 600 m long sea rocky cliff located at Sant'Andrea (Melendugno, South of Apulia, SE Italy) and faced to the southern Adriatic Sea. Here the cliff is made up of an about 15 m-thick sequence of laminate calcisiltites alternate with bioturbated calcarenites belonging to the Uggiano la Chiesa Fm. (Middle-Upper Pliocene).

The structural discontinuities detected with photogrammetry techniques were compared and validated with those derived from conventional in situ survey methods. Later on, the paper discusses assumptions and results of two- and three-dimensional finite element models developed to investigate the potential failure mechanisms of the sea cliff accounting for pre-existing weak planes or discontinuities with unfavourable orientation.

The failure mechanisms obtained by both FEM analysis agree well with those typically observed in the study area.

KEYWORDS Keywords: Sea cliff; Slope stability; UAV survey; ^gGeostructural setting; ^gGeomechanical survey; ^fFinite element model

1.1 INTRODUCTION

Rockfalls and rock sliding processes induce high risk conditions for communities and infrastructures located along the coastlines in terms of both people safety and exposed economy. Hence, advancements in the methodologies for hazard assessment of coastal rocky cliffs need to be developed. Nowadays, a significant support for the seamless modeling of rocky cliff structures is provided by the available advanced surveying methodologies. In particular, airborne LiDAR and Terrestrial Laser Scanning techniques, as well as close-range photogrammetry, calibrated by geostructural and geomechanical field surveys, represent powerful tools for detecting the three-dimensional geometry of rocky cliffs, as well as for characterizing rock joints and unstable rock portions (Westoby et al., 2012; Corsini et al., 2013; Mancini et al., 2013; Bemis et al., 2014; Cawood et al., 2017; Andriani and Parise, 2017 to mention a few). At places, manual field measurements can have limitations related to logistic difficulties, safety risks for the operators, and inaccessible sites. Moreover, manual surveys of discontinuities and structural patterns of the rock mass are

impracticable over large areas (Assali et al., 2014). In this perspective, manual surveys can provide information and guidance on how to set and calibrate the technical equipment available for 3D geometrical modeling of the rock masses studied, and check the results obtained applying the different aforementioned techniques.

Cawood et al. (2017) have proposed a state-of-the-art of the exploitation of LiDAR, Terrestrial Laser Scanner (TLS), compass-clinometer field measurements and close-range photogrammetry from Unmanned Aerial Vehicle (UAV) to improve the geostructural characterization of the area investigated and to increase the study area coverage. TLS and close-range photogrammetry can be also used to obtain dense 3-D point clouds for reconstructing three-dimensional geomechanical models and supporting deterministic numerical approaches aimed at assessing the cliff stability. However, for subvertical coastal cliffs overlooking the sea, earth-based methodologies such as LiDAR, TLS, robotic total station or terrestrial photogrammetry cannot be easily applied, as well as boat-based mobile laser scanning techniques are strongly limited by logistic constraints and coastal morphology (Michoud et al., 2015). Virtual dense representations of horizontal and subvertical surfaces of geomorphological features at cm-level of vertical accuracy and spatial resolution are spreading due to nadir and oblique photogrammetry with light UAVs and Structure from Motion (SfM) approach (Pike et al. 2017; Ružić et al., 2014). Use of small aerial vehicles in geoscience applications (Westoby et al., 2012; Mancini et al., 2013; Fonstad et al., 2013) allowed to explore the reliability of SfM-derived products (Agüera-Vega et al., 2016).

The use of UAV photogrammetry is founding increasing application for detailed reconstruction of subvertical rocky cliffs (James and Robson, 2012; Nex and Remondino, 2014; Genchi et al., 2015; Giordan et al., 2015; Warrick et al., 2016). However, the potentiality of advanced surveying techniques as input for geomechanical models is still rarely explored. Quinn et al. (2010) used TLS-based techniques to develop a two-dimensional finite-difference geotechnical modeling of a clay cliff. Ferrero et al. (2011) and Martino and Mazzanti (2014) applied TLS techniques to develop detailed limit equilibrium analyses of jointed rock cliffs. Applications of such methodologies in the geohazard investigation and landslide research have been also proposed by Riquelme et al. (2016), Abellan et al. (2016) and Balek and Blahůt (2017). Mancini et al. (2017) explored firstly the application of UAV-based surveys of a sea cliff in soft calcarenites to setup a three-dimensional numerical model for detailed stability assessment. However, this preliminary numerical model does not account for structural features existing in the rock mass and, hence, has been schematized as a continuum model, although joints have been recognized to exist and affect cliff stability. Recently, several authors explored the use of UAV-based photogrammetry to perform a geostructural analysis of rock masses, as an alternative to the conventional approaches that require field operations by geological experts (Ferrero et al., 2011; Assali et al., 2014; Bemis et al., 2014; Cawood et al., 2017; Piras et al., 2017). Some interesting applications of three-dimensional numerical modelling in rock stability, specifically by means of distinct element methods, can be found in the literature (Brideau et al., 2011, 2012), although in these cases a schematized topography of the rock slope has been assigned in the analyses.

In this paper a structured methodological approach to assess hazard of coastal rock cliffs, characterized by discrete joints, based on the application of three-dimensional finite element models (FEM) that implement the structural information derived from images acquired by Unmanned Aerial Vehicles (UAV) and validated by traditional in-situ geostructural and geomechanical surveys, is proposed. Therefore, the procedure here proposed is based on three main steps, as follows: 1) description of the cliff surface geometry in detail as obtained from a UAV survey, 2) detection of main joints existing in the rock mass by means of the integration of UAV and traditional geostructural surveys and 3) building of three-dimensional finite element model for cliff stability assessment, where all the information gathered from the previous steps are introduced and possible hazard scenarios can be simulated. Since the work proposed by Mancini et al. (2017) deals with hazard assessment of rocky cliffs mainly treated as continuous, e.g. with no discontinuities, this paper specifically focuses on the role of discrete structural joints in the control of cliff stability and potential failure mechanisms of the rocky cliff, the techniques that can be adopted to identify discontinuities in similar situations and the numerical techniques that can be adopted to take into account their presence. In this perspective, the main assumptions made in the methodology are as follows: the cliff surface should be bare and free of vegetation; the number of discontinuities should be limited; most of the cliff surface should be above the sea level, with only a small portion submerged.

As a test case study, a 600 m long sea cliff along the southern Adriatic Sea (Fig. 1; Sant'Andrea, Melendugno, Apulia - Italy) was surveyed by UAV photogrammetry and, later on, a 3-D finite element model was setup on a specific cliff sector. The study area is represented by a plunging cliff, where in-situ surveys were performed only in the cliff lateral areas and on the platform at the top of the cliff. This is a common situation along the coastline rocky cliffs, so that UAV can represent the unique instrument to acquire information about joint features. Hence, a 3D surface from UAV photogrammetry that fits the requirements for the geomechanical modeling has been developed and the main structural features of the rock mass have been detected with the same technology for a limited part of the extensive morphological data. Then, the structural joints detected with photogrammetry techniques were compared and validated with those derived from conventional survey techniques. Later on, a detailed characterization of the physical and mechanical properties of the soft calcarenites forming the examined cliff is presented. Finally, the paper discusses assumptions and results of a three-dimensional finite element model developed to investigate the potential failure mechanisms of this portion of the sea cliff accounting for pre-existing weak planes or discontinuities with unfavourable orientation.



Figure 1. Fig. 1 Frontal view of the sea cliff at Sant'Andrea (Melendugno, Apulia - southern Italy).

alt-text: Fig. 1

2.2 ~~PROPOSED~~ proposed methodology

Stability assessment of jointed rocky vertical cliff is not a straightforward task, since several factors do affect the same problem, such as the cliff three-dimensional geometry, both at small as well as at local scale, the three-dimensional structural setup, the physical and mechanical properties of the rock matrix, the mechanical properties of the rock joints, the erosion rate at the cliff toe, the effect of the environmental weathering acting on the whole rocky cliff (i.e. sea salt, sea spray, rainfall water infiltration, wind erosion, etc.) and the consequent degradation of the rock and joint material properties (Ciantia et al., 2015), to mention the most important ones.

Accordingly, in this section a comprehensive methodology for the assessment of the stability of a coastal cliff is proposed, as follows (Fig. 2):

1. Detailed three-dimensional geometrical survey of the cliff by means of UAV-based photogrammetry techniques;
2. Detection of the most relevant fractures and joint sets by means of the analysis of UAV models;
3. Geological, geostructural and geomorphological analysis of the cliff by means of in-situ surveys and assessment of the typical failure mechanisms taking place along the cliff; this stage can be also used to validate the results of the previous step (step 2); conceptual models can be useful at this stage in order to investigate the more relevant failure mechanisms and the role of specific factors on them;
4. Laboratory tests on samples taken from the same rock mass and assessment of the main rock and joint physical and mechanical properties; this stage of the procedure can be also aimed at assessing the effects of saturation, or eventually environmental weathering acting along the cliff.
5. Processing and meshing strategy of the cliff surface point cloud, as detected from UAV survey, and importing into a 3-D finite element model;
6. Setup of the 3-D numerical model, choice of the assumptions, processing and analysis of the results. To this purpose, the model should incorporate the most important fractures detected in the rock mass.

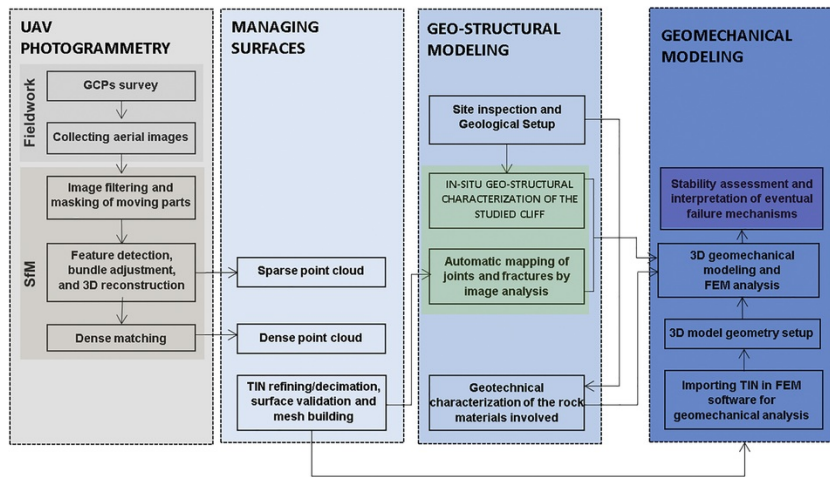


Figure 2. Fig. 2 Workflow of the methodology adopted in the stability analysis of the cliff.

alt-text: Fig. 2

In this scheme, several differences and advancements are proposed with respect to the work proposed by Mancini et al. (2017), the latter being mainly based on continuous rock mass assumptions. In particular, points 2 and 3 represent an upgrade of the methodology, since a specific work is required to detect the main joints existing in the rock mass by means of an integration of both UAV-derived 3-D surface and traditional field surveys. Moreover, some investigations on the strength properties of the cementation filling the discontinuities should also be carried out. Finally, point 6 represents also an important advancement with respect to the methodology proposed by Mancini et al. (2017), since in this case the 3-D FEM model should account for the main joints influencing the rock mass behavior by means of interface elements, as described in detail later on.

Some more details of the aforementioned methodological steps are here proposed.

As regards steps 1 and 2, in this paper, the 3D cliff discontinuity planes was reconstructed by nadir and oblique photogrammetry by using a light UAV (Unmanned Aerial Vehicle) model and the Structure from Motion (SfM) approach to image processing, which proved to be very suited to the representation of horizontal and subvertical faces of geomorphological features at cm-level of vertical accuracy and spatial resolution (Westoby et al., 2012; Bryson et al., 2013; Mancini et al., 2013; Fonstad et al., 2013; Agüera-Vega et al., 2016). In fact, when the reconstruction of sub-vertical coastal rocky cliffs in front of the open sea is required, the absence of vantage points for surveys with different terrestrial methodologies could represent a main limitation. Clear advantages in using UAV-based surveys of coastal cliffs are suggested in recent papers (Warrick et al., 2016; Cawood et al., 2017; Mancini et al., 2017). A semi-automatic extraction of discontinuities allows to reduce efforts in the in-situ geological surveys whenever the investigated areas pose logistic problems related to the operator safety and inaccessible sites. The proper identification of discontinuities needs 3D models for representing the surface complexity at the required spatial scale (Cracknell et al., 2013; Riquelme et al., 2016). The strategy adopted for the surface 3D reconstruction may affect the obtainable results in terms of noise and spatial resolution. Among the geometric parameters involved in the surfaces characterization and discontinuities extraction, curvature is very often adopted as basic property to highlight areas of a surface in which the greatest slope rate is focused (Rutzinger et al., 2007).

In step 3, the description of the rock masses was based on the procedure suggested by ISRM (1981), starting from a geological and geomorphological survey aimed at building a base map (Fig. 3), showing rock unit distribution, stratigraphic and structural details, and an appropriate engineering-geological model for predicting the instability of the cliff and reconstructing the geometry and potential kinematic evolution of mass movements. Particular emphasis was given to the characteristics of discontinuities and also to degree of rock weathering, as they have a strong influence on the engineering behavior of carbonate rocks. Orientation, spacing, persistence, roughness, aperture, filling, number of sets, state of weathering, water conditions and parallelism between joint and cliff strikes were evaluated. In addition Slope Mass Rating (SMR) (Romana, 1985 and references therein) and Cliff Instability Susceptibility Assessment (CISA) (Andriani and Pellegrini, 2014) were used for the rock mass classification along the studied coastal stretch and for qualitative assessment of the sea cliff instability susceptibility at a given scale.



Fig. 3, Fig. 3 Lithologic map of the study area with stereonet (lithologic cross-section in Fig. 5).

alt-text: Fig. 3

For step 4, following the standard test procedures proposed by [ISRM \(1979\)](#), rock physical properties were determined on rock samples. Uniaxial compressive strength and indirect tensile strength (Brazilian) tests, under both dry ($\sigma_{\text{dry}}, \sigma_{\text{tdry}}$) and saturated state ($\sigma_{\text{csat}}, \sigma_{\text{tsat}}$), were also carried out according to [ISRM \(1978, 1979\)](#). The post-peak response of the rock material was observed during the tests by using a servo-controlled testing machine for dry and saturated samples ([Lollino and Andriani, 2017](#)). Later on, the GSI for carbonate rock masses (Geological Strength Index, [Marinos and Hoek, 2001](#)) and the generalized Hoek-Brown failure criterion were used and the equivalent Mohr-Coulomb parameters were evaluated ([Hoek and Brown, 1980](#); [Hoek et al., 2002](#)).

In Step 5, the SfM general workflow is used to process the dataset of nadir and oblique images for data import, image alignment, creation of the sparse cloud, refinement of image alignment and dense image matching in a single adjustment procedure ([Rupnik et al., 2014](#); [Rossi et al., 2017](#)). The SfM approach is useful to generate the 3D sparse point cloud by the simultaneous estimates of internal parameters, camera positions and object coordinates. The initial search for conjugate points (matching features in multiple images) is performed by the scale-invariant feature-transform algorithm ([Snavely et al., 2006](#); [Lowe, 2004](#)), while the successive bundle adjustment step is aimed at refining such parameters by an iterative process. Such parameters are used by the dense matching algorithms to create a dense point cloud ([Hirschmuller, 2008](#)). The dense point can be converted into a surface by a meshing procedure based on the TIN (Triangulated Irregular Network) approach. In particular, among the possible TIN-based strategy for meshing, the method proposed by [Schumaker \(1993\)](#) can be preferred because of the ability to provide polygonal or polyhedral approximation of the desired object by generating poly-faces, the triangles, which follow the geometric shape of the point cloud.

Step 6 is devoted to the setup, processing and results interpretation first with the two- and then with the three-dimensional numerical models. Nowadays, three-dimensional numerical models represent efficient tools to investigate boundary value problems and are necessary when the problem cannot be schematized by means of a two-dimensional model in terms of geometry, boundary and loading conditions, as for example rocky cliffs characterized by complex geometries or stress-strain conditions not represented by plane-strain assumptions. In this perspective, three-dimensional FEM models can be helpful to assess the global failure mechanism eventually involving the whole cliff as well as local rock collapses of the rock cliff. Moreover, three-dimensional numerical analyses allow to account for the presence of certain number of layer surfaces and discontinuities with their own geometry by means of the introduction of interface elements with properties representative of the joint mechanical behaviour. The mesh discretization should be consistent with the point cloud resolution and a small element size should be chosen in the domain area where high stress and strain gradients are expected.

3.3 Case study: the sea cliff of Sant'andrea, Melendugno

3.1.3.1 Typical coastal instability processes in the study area

The study area is located on the Adriatic side of the Salento peninsula marked by a landscape of narrow and low-elevated carbonate ridges which separate small plains shaped on Pliocene and Quaternary sediments. In particular, the coastal stretch examined is situated in a tectonically uplifting area with a generally indented development and a series of caps and inlets, arches, stacks and a small bay where an ephemeral water channel slightly incised reach the sea ([Fig. 4](#)).

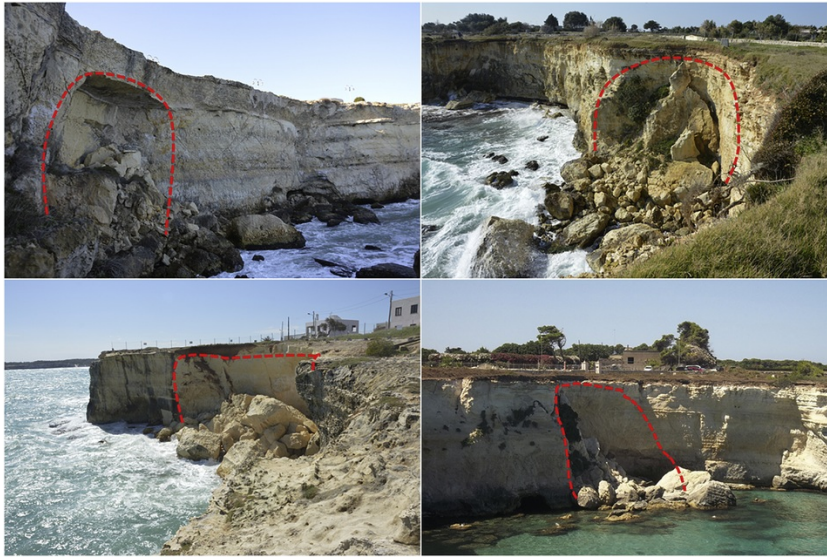


Figure 4. Fig. 4 Rock blocks detached from the sea cliff, caps, inlets, arches and stacks in the area of Sant'Andrea.

alt-text: Fig. 4

Inlets, small bays and sea caves are located along structural weaknesses, typically along faults. The area is characterized by the presence of a steep plunging cliff, with a vertical and, in places, overhanging face. The cliff ranges from 12 to 18 m in height and ends in subhorizontal surfaces at the top, whereas the cliff foot is below the sea level at 1–2 m depth. The roof of the cliff lacks recent covering deposits due to wave splashing and weathering processes that are also responsible for rock mass decay.

The cliff develops in well-stratified fossiliferous yellowish marly calcisiltites and yellowish to light grey calcarenites belonging to the Middle-Upper Pliocene Uggiano la Chiesa Fm. whose type area corresponds to the coastal stretch between San Foca and Otranto.

Selective erosive phenomena and landsliding along the coastline are widespread, even though cliff recession is essentially an episodic and localized process closely associated with storm waves. The study area is, in fact, characterized by a low seismicity. Here the recorded earthquakes came from neighbouring zones (northern Apulia, southern Apennines, Adriatic and Ionian sea, Albania and Greece) so that a seismic event can rarely provoke a landslide. Slides, falls and topples characterize the coastal cliff stretch. Generally, the detachment occurs along tension cracks controlled by stress release at places along faults, parallel to the coastline and steeply inclined, whereas deep notches give rise to rock slides locally evolving into block falls, followed by free fall of the debris. Similar tension features are frequent and indicate that other mass movements of the same type are likely in the near future. Rock falls occur where there are sea caves and overhanging blocks due to wave undercutting. A joint sets striking obliquely across the cliff face determine a high degree of freedom for block movement. The development of the caves is due to the erosive and corrosive forces of sea water flow on the cliffs; the action of these forces is more effective along persistent joints affected by karst, especially, in correspondence with the mixing zone between freshwater and saltwater. Toppling is common where calcarenites or calcisiltites have a notch between high and low tide levels and where tension cracks dip steeply landward. The probability of landslide occurrence depends on the ratio of the depth of undercutting at the cliff base and the distance of the tension cracks from the cliff face. At places, the presence of a notch, the width of which is greater than the depth, and of a tension crack set close to the cliff top edge constitute an important indicator of slope failure hazard induced by cyclic wave action. Arches and stacks are aligned NW-SE along the major trending normal faults in Apulia, thought to be due to the foreland response to the northeastward thrusting of the Apennine chain (Del Gaudio et al., 2007). Stacks are produced by the collapse of the vault of sea arches and represent the last phase of the landform erosive evolution model “cave-arch-stack”, due to the continuous wave action along structural weaknesses.

Rock mass strength is controlled by discontinuities and mechanical properties of intact rock blocks. Reduction in rock mass strength is due to weathering and fatigue caused by cyclic loading of waves at the cliff base. The weathering processes include carbonation, salt weathering, thermal deterioration, water layer weathering (associated with the wetting and drying process) and biological weathering, especially by boring organisms. The assailing forces of wave depend on the wave energy, in turn depending on wind strength and duration, water depth and density, and fetch. The intensity of erosive forces controlling failure mechanisms is determined by the wave type

immediately in front of the cliffs and this is determined by the relationship among offshore wave characteristics (wave height, wave angle and wave period), tidal condition and nearshore submerged morphology.

3.2.3.2 Geological model

The outcrop of the cliff studied is formed in a 15 m-thick sequence of laminate calcisiltites alternate with bioturbated calcarenites rich in bivalves, red algae, benthic foraminifers and bryozoans belonging to the Uggiano la Chiesa Fm. (Middle-Upper Pliocene). It is a well-stratified sequence of yellowish marly sediments with yellowish to light grey low cemented biocalcarenites in which at places there are centimeter-scale well cemented biotrital limestones, also called “catine” from the quarrymen of the surrounding areas. The Uggiano la Chiesa Fm. lies unconformably on older geological units, but the transgressive surface is not displaced along the sea cliff.

Generally, the biocalcarenite facies prevails in the lower and higher parts of the cliff, while in the middle one the marly calcisiltites are predominant (Fig. 5). Topography on the cliff top is flat, as on a marine terrace, and stratification as well as lamination are sub-horizontal. Widespread patterns of bioturbation, represented mainly by horizontal burrowing trace fossils, can be observed on the cliff top and in the biocalcarenite facies, especially where the concentrations in fossil bivalve shells is higher.

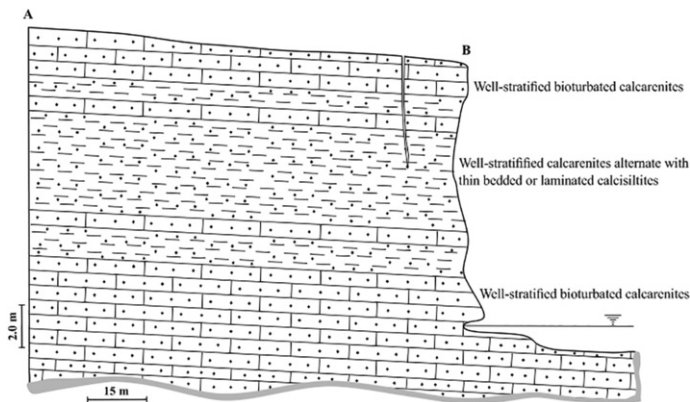


Figure 5. Fig. 5 Lithological cross-section of the Sant'Andrea cliff (A-B section trace in Figure 3).

alt-text: Fig. 5

The geostructural setting of the cliff is mainly given by three major (S0/J1, J2, J3) and two minor discontinuity sets (J4, J5) which were grouped in three distinct structural fracture domains, associated with the structural, tectonic and geomorphic evolution of the study area. The mean orientation of each discontinuity set together with other parameters were identified in the study area based on field measurements (Table 1). The joint set S0/J1 represent the bedding planes within the rock mass along the cliff; it strikes N0-10W and dips 0°-10° towards E. J2 strikes N55-70W and dips 80°-90° towards NE, while J3 strikes N20-40E and dips 80°-90° towards SE. J4 shows N-S, NNE-SSW trends (N0-5E) and dips 70°-90° mainly towards E, while joint set J5 strikes N80-90E or N80-90W and dips 60°-80° towards NNE. Near-horizontal bedding-planes constitute a distinct joint set, while J2 and J5 fall into the same structural domain (“Apenninic system”); at the “anti-Apenninic” system belong J3 and J4 sets. During the field measurements, unfortunately, it was not always possible to make a distinction between faults and tension fractures because the main orientation of the rocky cliff is strongly controlled by the structural pattern and tectonic setting. Thus, tension fractures commonly occur along pre-existing faults and fractures related to the tectonic evolution of the entire area.

Table 1. Table 1 Main parameters of the discontinuity sets identified by the authors in the study area.

alt-text: Table 1

Discontinuity set	Mean attitude	Trace length (m)	Large roughness (metre scale)	Aperture (cm)	Spacing (m)
S0/J1	95/5	10–20	Planar smooth	0–0.5	0.30–1.50
J2	30/85	5–15	Slightly undulating	0.3–20	3–10
J3	120/85	3–10	Slightly undulating	0.3–10	3–10

J4	90/80	3-10	Moderately undulating	0-1.0	>6
J5	0/70	3-15	Planar rough	0-2.0	>6

In general, they are normal to left-lateral oblique slip faults. Particularly, NW-SE and E-W faults show evidences of oblique reactivation and clear surface ruptures, exceeding 10 m in length, cm to dm wide apertures but commonly limited fault throw ~~less than~~ ≤ 0.5 m is visible. Probably, this fault system is older than the one N-S or NE-SW oriented and it seem to have been reactivated by the latter. Discontinuities are dry but shows evidence of water flow such as staining, leaching and vegetation or contains damp filling, but no free water is present. Open discontinuities are at places filled with soft sandy or residual materials and the joint interfaces are mostly moderately rough, at small-scale, and moderately or slightly undulating at large-scale. Wide apertures characterize the discontinuities oriented approximately parallel to the coastline, probably controlled by stress release but at places located along tectonic lineaments. Totally or partly healed and re-cemented discontinuities develop landward, far from the cliff edge, or are oriented transversally with respect to the coastline. Discontinuities are extremely (true spacing ~~greater than~~ ≥ 3 m) or very widely spaced (1 to 3 m) and only close to the cliff edge the spacing becomes lower.

3.3.3.3 Geotechnical characterization of the intact rock materials and rock masses

The rock materials cropping out along the cliff at Sant'Andrea belongs to two different lithofacies according to the stratigraphic sequence of calcisiltites and biocalcarenites as described in the previous section (Fig. 5). Each lithofacies constitutes de facto a geotechnical unit, quite different from the other in terms of physical properties and mechanical behavior, strongly conditioned by depositional fabric and diagenetic processes, but not for chemical and mineralogical composition because they are both carbonate-rich units. This implies heterogeneity in the rock masses along the cliff under the influence of differentiated erosion and weathering processes due to textural and structural features. In fact, the calcisiltites exhibit more susceptibility to erosion and degradation, both at the meso-scale and the macro-scale, than calcarenites and at places the instability mechanisms are just controlled by the contrast in shear strength and stiffness between the two units.

Laboratory tests were performed on samples taken from an open-pit quarry located about 600 ~~meters~~ from the study site. In particular, dry unit weight, saturated unit weight, porosity, water absorption, degree of saturation, uniaxial compressive strength and indirect tensile strength in the dry and saturated states respectively for cylindrical (diameter $d = 60$ mm; height $h = 140$ mm) and disk (diameter $d = 60$ mm; height $h = 30$ mm) samples were measured. According to [Andriani and Walsh \(2010\)](#) ~~(Please correct with: Andriani and Walsh (2002; 2010))~~ water absorption and degree of saturation (Sr) were evaluated on specimens immersed and suspended in distilled water at 20°C for 48 h and then saturated completely under vacuum (80 kPa) without removing them from the water basket. As regards the specific gravity (Gs), reference was made to a value of 2.71 on the basis of the chemical composition of the rocks.

Concerning the calcarenite unit, dry unit weight ranges between 14.5 and 17.0 kN/m³, whereas the saturated unit weight is between 18.9 and 20.5 kN/m³. Porosity is in the range 36% ~~45%~~, water absorption between 20.8% ~~30.4%~~ and degree of saturation is 100% showing that pores in the rock particle systems are interconnected and continuous, so that the porosity is supposed to be effective. Uniaxial compressive strength under dry conditions ranges approximately between 5 and 10 MPa, whereas under saturated conditions strength lies in the range between 2 and 2,5 MPa (Fig. 6). Indirect tensile strength under dry conditions ranges between 220 and 310 kPa and under saturated conditions is between 90 and 140 kPa.

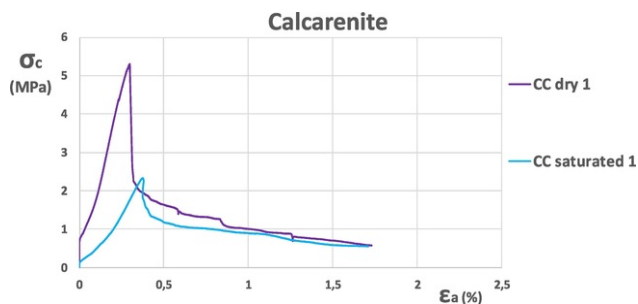


Figure 6. Fig. 6 UCS stress-strain curves for the calcarenite samples obtained from the same rock block.

alt-text: Fig. 6

Based on the uniaxial compressive strength at the dry state, the calcarenite examined can be classified as moderately soft according to the classification proposed by [Andriani and Walsh \(2010\)](#) and weak according to the ISRM one (1978). Based upon the aforementioned values, the shear strength parameters according to the Mohr-Coulomb failure criterion under saturated conditions were derived through a linearization of the Hoek & Brown failure envelope by assuming a GSI = 90, which is typical of massive and intact rock, and $m_i = 10$ ([Cai, 2010](#)). In particular, assuming a stress range representative of the in-situ stress levels, the resulting shear strength parameters are in the following

ranges: $c' = 200\text{--}300$ kPa and $\phi' = 28\text{--}35^\circ$. A significant influence of the saturation degree on the modulus of elasticity, measured at 50% of the uniaxial strength (E_{50}^u), was also measured, with values ranging from 1000 to 2000 MPa, at the dry state, and from 300 and 1500 MPa, at the saturated state.

As regards the calcisiltite unit, dry unit weight ranges between 11.5 and 13.5 kN/m³, whereas the saturated unit weight is between 17.1 and 18.3 kN/m³. Porosity is in the range 49%–57%, water absorption between 35.7%–48.5% and degree of saturation is 100% also for this unit. Uniaxial compressive strength under dry conditions is in the range between 1 and 2 MPa and under saturated conditions is between 0.3 and 0.4 MPa (Fig. 7). Indirect tensile strength under dry conditions ranges between 120 and 140 kPa and under saturated conditions is between 45 and 52 kPa. A strong reduction of UCS and ITS larger than 50% was observed for the saturated samples with respect to dry samples, and this is compatible with a scarce and irregular presence of calcite cement and a grain-size distribution with a fine tail. Based on the uniaxial compressive strength at the dry state, the calcisiltite examined can be classified as extremely soft according to the classification proposed by Andriani and Walsh (2010) and very weak according to the ISRM one (1978). Similarly, the shear strength parameters were evaluated according to the Mohr-Coulomb failure criterion under saturated conditions through a linearization of the Hoek & Brown failure envelope. Also for this unit GSI = 90 and $m_i = 10$ were adopted. In particular, assuming a stress range representative of the in-situ stress levels, the resulting shear strength parameters are in the following ranges: $c' = 50\text{--}150$ kPa and $\phi' = 26\text{--}34^\circ$. The modulus of elasticity, measured at 50% of the uniaxial strength (E_{50}^u), was also measured, with value equal approximately at 330 MPa, under dry conditions, and ranging from 100 to 300 MPa, under saturated conditions.

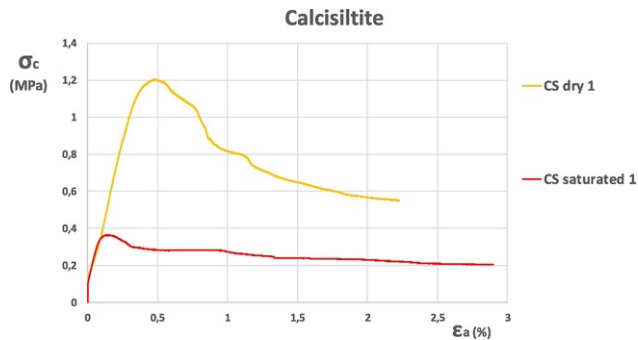


Figure 7. Fig. 7 UCS stress-strain curves for the calcisiltite samples obtained from the same rock block.

alt-text: Fig. 7

According to Slope Mass Rating (SMR = 26–38) (Romana, 1985) the rock mass belongs to the class described as “bad”, the cliff is defined “unstable” and the probable failure modes are topples, falls and slides down an inclined plane. As a result of the analysis of the data obtained from the applications of the CISA method (CISA = 42–58) (Andriani and Pellegrini, 2014), it was found that the coastal stretch of Sant’Andrea is “unstable”, although at places retreat processes are not visible.

3.4.3.4 Automatic mapping of joints and fractures by image analysis

In order to investigate the potentialities of image analysis to detect the main geosstructural features, the cliff was surveyed by means of combined UAV nadir and oblique photogrammetry. The UAV surveys was selected due to the absence of useful points for alternative terrestrial surveys and were performed by means of a hexacopter ESAFLY A2500 (designed and manufactured by SAL Engineering, Italy) equipped with a Canon EOS 550D digital camera (focal length: 25.0 mm; sensor resolution: 5184 × 3456) and navigation-grade GNSS receiver. Using such configuration the airframe guarantees a flight endurance of at least 20 min. Three flights with parallel flight lines were performed at an altitude of 50 m a.g.l. and nadir captures were taken at a rate of one shot per second, resulting in 541 images acquired with a forward and side overlap of 90%. The vertical portion of the sea cliff required 530 additional oblique images acquired by a flight line parallel to the cliff profile at an average distance of 20 m. During the preliminary processing steps the images affected by blurring or acquired under unfavorable/unfavourable attitude were filtered out. An accurate georeferencing was obtained by 13 distributed ground control points (GCP) surveyed through GNSS receivers and a static relative GNSS positioning. Baselines between two permanent GNSS stations belong to the Apulian GNSS positioning facility and local GCPs were used for such a purpose. The standard deviation of final positioning of GCPs was at least of 1 cm.

The UAV images were processed using the photogrammetric workflow as discussed in the methodology section (see step 5) and the final dense cloud generated. In order to comply with the limitation imposed by the geomechanical modeling tool, a procedure able to reduce the file size without affecting significantly the surface properties and complexity has been assessed. The optimization/refinement procedure used in this work to reduce the dense cloud and generate a reliable three-dimensional model that preserved the full descriptive capacity of the original surface a criterion was selected. In particular, a decimation algorithm able to take into account the local surface curvature was used. Such an algorithm will preserve surfaces with higher curvature trend by applying a lower reduction ratio and the principal geological structures of the rock mass and their orientation will be better represented.

More details about limitations and accuracy of decimation procedures applied to the same dataset at 4% and 1% of the full resolution could be found in [Mancini et al. \(2017\)](#). In this study, the discontinuities extraction was performed by means of algorithms belonging to the fields of 3D modeling and reverse engineering ([Buonamici et al., 2018](#)) that basically allow the extraction of discontinuities according to surface curvature. Firstly, low curvature areas are detected into the 3D surface model and divided in regions ([Fig. 8a](#)). Regions constitute a segmentation of the original surface and contours between them are then vectorized in lines that constitute real discontinuities ([Fig. 8b](#)). The ability of the method to distinguish discontinuities is related to the ability and reliability in curvature detection. Noise and small roughness in the surface may generate errors in discontinuities extraction; here, the use of a decimated mesh (1% of the original size) as described by Mancini (2017), ensured the removal of effects of low and sparse vegetation and others 'non-geological' elements. Authors explored tools and methods implemented within Geomagic Studio 2013 suite. The extract region command allowed to set up sensitivity to curvature and the wideness of contour between regions for a precise definition of flatness areas and extraction of discontinuities. Discontinuities can then be exported as .iges or .dxf files and easily employed for further analysis.

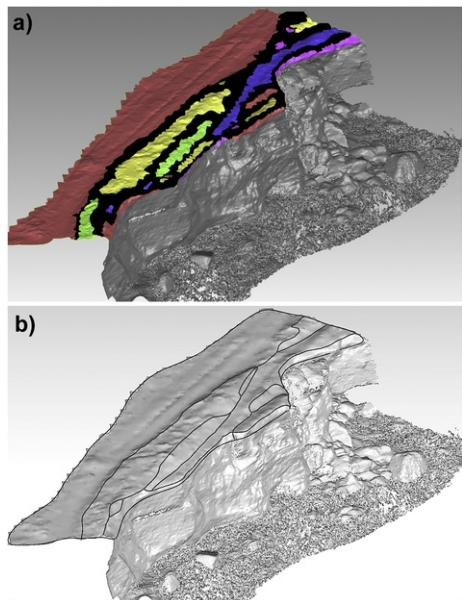


Figure 8. Fig. 8 a) Extract regions utility: extraction of flat regions (colored areas) and separators (red strips); b) Contour utility, generation of contour lines. [\(For interpretation of the references to colour in this figure legend, the reader is referred to the web version of this article.\)](#)

alt-text: Fig. 8

[Fig. 9](#) shows an orthophoto of the study area, with the indication of the discontinuities automatically defined by means of the 3D UAV-based model (blue lines) as well as the main discontinuities detected according to the in-situ survey (yellow lines). The results obtained from the automatic mapping here proposed are seen to be consistent with those derived from the conventional in-situ geosurvey.

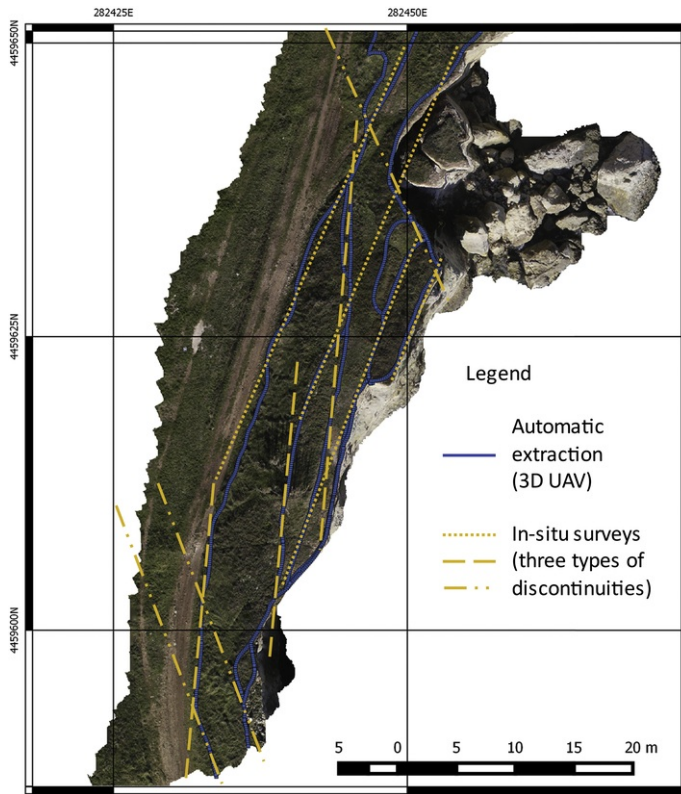


Figure 9. Map of detected discontinuity lines. Discontinuities automatically detected through 3D UAV model (blue), discontinuities derived by a field surveys (yellow). [\[For interpretation of the references to colour in this figure legend, the reader is referred to the web version of this article.\]](#)

alt-text: Fig. 9

3.5.3.5 Two-dimensional finite element model

In order to investigate the role of the sea erosion at the cliff foot and that of a vertical joint parallel to the cliff front in the cliff stability, a two-dimensional finite element model of an ideal 12-m high cliff was performed [with the numerical code PLAXIS 2D \(PLAXIS-BV, 2018\)](#) to serve as conceptual model of the cliff behavior. In particular, the numerical domain and the discretization mesh adopted in this analysis is shown in [Figure 10](#). Soft calcarenite is here considered an elastic perfectly-plastic Mohr-Coulomb medium, with a cohesion $c' = 150$ kPa, a friction angle of $\phi' = 30^\circ$ and a tensile strength of $\sigma_t = 150$ kPa. Since the rock mass has been considered for sake of simplicity as homogenous, the mean values of the geotechnical parameters, e.g. shear strength and unit weight, previously identified for the two different units have been used.

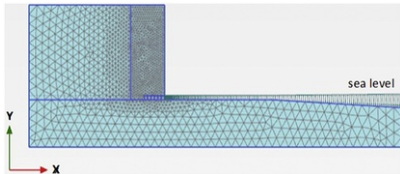


Figure 10. 2-D model with sea erosion at the foot (no joint interface activated): Numerical model with discretization mesh

alt-text: Fig. 10

The results of a first continuous model (no vertical interface activated) implementing two different sea erosion depths at the cliff foot, respectively of 1 and 3 m, indicate that no signs of on-going failure processes is observed, even with a 3-m depth erosion, so that the cliff remains stable.

When reduced rock mechanical properties are introduced in terms of a lowering of both the cohesion and the tensile strength values ($c' = 50$ kPa and $\sigma_t = 50$ kPa) in order to simulate the effects of rock weathering along the cliff, even with a 1-m depth erosion at the foot, the numerical model does not converge. In this case, a failure mechanism indicated by an oblique shear band starting from the end of the erosion depth and evolving towards the top of the cliff, at a distance of about 5–6 m from the crest, is calculated (Figure 11). (See Fig. 12.)

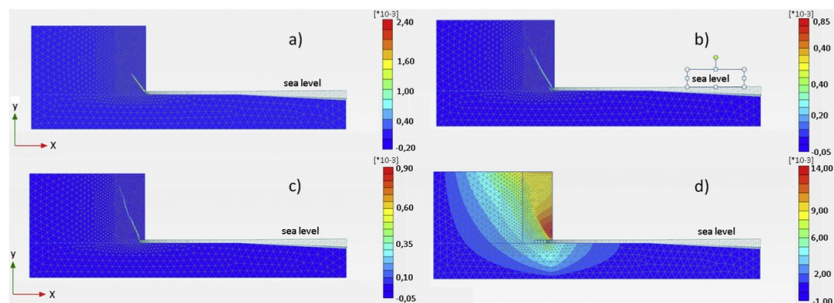


Figure 11, Fig. 11 2-D model with sea erosion at the foot (no joint interface activated) and reduced rock mechanical properties due to weathering: a) deviatoric strain γ_s without erosion at the cliff foot; b) deviatoric strain γ_s with erosion depth at the cliff foot of 1 m; c) deviatoric strain γ_s with erosion depth at the cliff foot of 3 m; d) total displacements u_x with erosion depth at the cliff foot of 3 m.

alt-text: Fig. 11

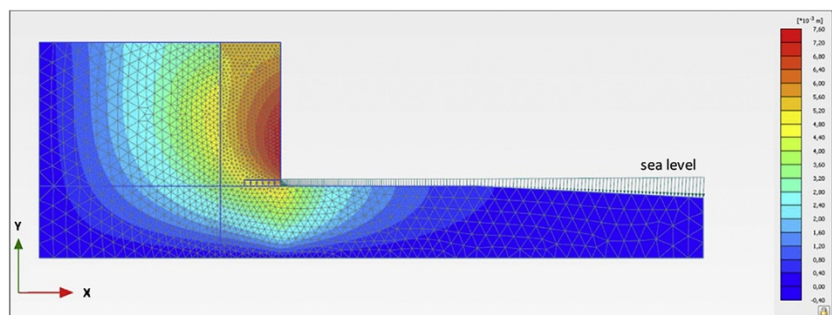


Figure 12, Fig. 12 2-D model without sea erosion at the foot and joint interface activated (no rock weathering): total displacements u_x .

alt-text: Fig. 12

The simulation of a vertical joint (i.e. parallel to the cliff face) has been then simulated by implementing a vertical interface at a distance of 5 m from the edge. In particular, when the vertical joint is characterized by $c' = 0$ kPa, $\phi' = 30^\circ$ and $\sigma_t = 0$ kPa, the numerical model does not converge, even with no erosion at the foot and assigning unweathered mechanical properties of the rock, and a failure mechanism involving the cliff portion up to the interface is observed (Figure 12 19 (this is the citation of figure 12) (here) (This is figure 12 and not Fig.19)). Instead, when a slight cementation degree of the joint is assumed ($c' = 10$ kPa, $\phi' = 30^\circ$ and $\sigma_t = 10$ kPa) and no weathering is considered for the intact rock, no failure process is observed, unless an erosion depth of 1 m is simulated in the model. Finally, adding the simulation of rock weathering (rock mechanical degradation), under the same previous assumptions, the model indicates a failure mechanism connecting the end of the erosion depth to the interface joint, already when an erosion depth of 0.5 m is simulated (Figure 13).

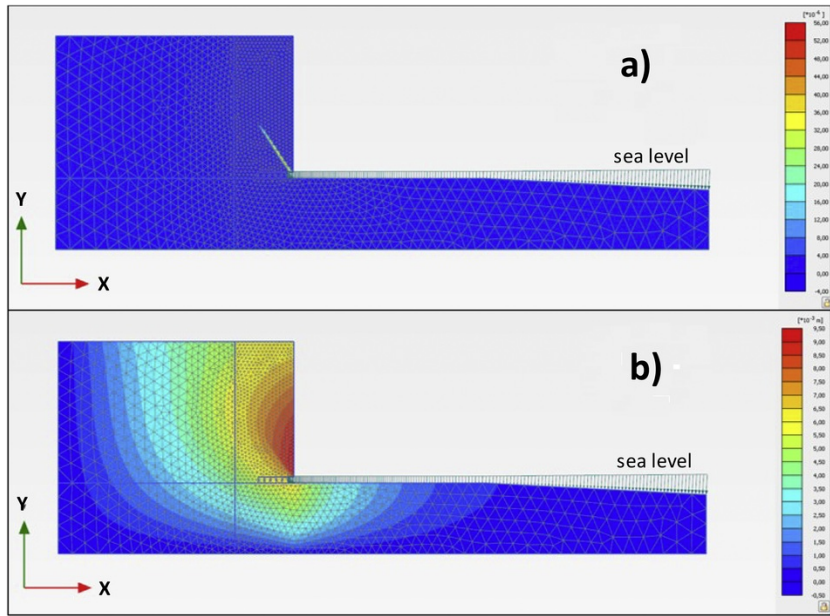


Figure 13. Fig. 13 2-D model with sea erosion at the foot, slightly cemented joint interface activated and reduced rock mechanical properties due to weathering: a) deviatoric strain γ_s ; b) total displacements u_x .

alt-text: Fig. 13

The results of this two-dimensional model indicate that the cliff failure is generally the consequence of a combination of different factors, as the foot erosion, the existence of re-cemented joints in the rock mass and their mechanical strength, the mechanical weathering of the intact rock, which can all interact to generate the loss of equilibrium of the cliff.

3.6.3.6 3-D finite element Analyses: model setup, assumptions and results

The three-dimensional analysis domain has been built by importing in Plaxis-3D FEM code (PlaxisLAXIS:BV, 20173) the TIN surface of the cliff sector shown in Figure 8 at 1% of the full resolution; the three-dimensional solid is shown in Figure 14. Later on, the domain was completed by extruding the cliff surface in the x-direction and adding a rock volume below the sea surface according to the bathymetry in the same area. Vertical side boundaries have been imposed to delimit the numerical domain in the horizontal plane, whereas a horizontal surface has been assigned both at the top of the cliff, to simulate the horizontal plateau, and at the base of the model. The structural joints subparallel to the cliff face, as defined in situ from the geostructural analysis, have been simulated in the FEM software through the implementation of structural elements called interfaces. Interfaces are mesh-less elements that have been used in our analyses to identify rock discontinuities, although providing numerical continuity between two adjacent solids. The three-dimensional mesh is formed of 40,000 tetrahedral elements as a result of a compromise between numerical accuracy and computational costs, with the number of nodes forming the 3D domain equal to 300,000 (Fig. 15). In particular, a very fine mesh (average element size = 0.40 m) has been used for the volume close to the cliff surface, whereas a significantly coarser mesh (average size = 2.7 m) has been adopted for the remaining portion of the model, further from the cliff surface. The finite element model was aimed at exploring the areas of the rock cliff prone to the onset of rock failure as well as the failure mechanism that typically occur within these rock masses characterized by the interaction between intact soft rocks and a small number of joints. The intact calcarenite rock material has been assumed to behave according to a Mohr-Coulomb elastic-perfectly plastic model, with non-associated flow ($\psi = 0^\circ$) and tension cut-off. A Mohr-Coulomb law, defined by specifying both the cohesion value and that of the available friction angle along the discontinuity surface, has been also used for the interfaces. The specific parameters adopted in the numerical model below described according to the data presented in the previous section are listed in Table 2. Two stages of analysis have been assigned in the model: in phase 1, the initial stress state has been prescribed to the domain by means of a gravity loading procedure; in phase 2, the rock material is instead supposed to behave according to an elasto-plastic constitutive model in accordance with the assigned parameters. As regards intact rock, while the friction angle value has been kept as fixed, the cohesion value has been set as variable in order to derive the conditions that typically give rise to the collapse of the cliff as well as the corresponding mobilized cohesion value. This simulation is aimed at reproducing numerically the process of loss of cementation which typically takes place within the soft calcarenites studied as a consequence of the environmental weathering that, in the specific case study, occurs in terms of rainfall infiltration, sea-salt action and wave action. Therefore, rock cohesion was gradually reduced from values of $c = 150$ kPa, which is here chosen as a representative value of both the two facies of the rock formation examined, i.e. calcarenite and calcisiltite, under saturated conditions, to a very low value of

50 kPa. Concerning the joint mechanical behavior, fractures were initially considered as uncemented, with values of cohesion and tensile strength of the corresponding interface close to zero (Table 2).

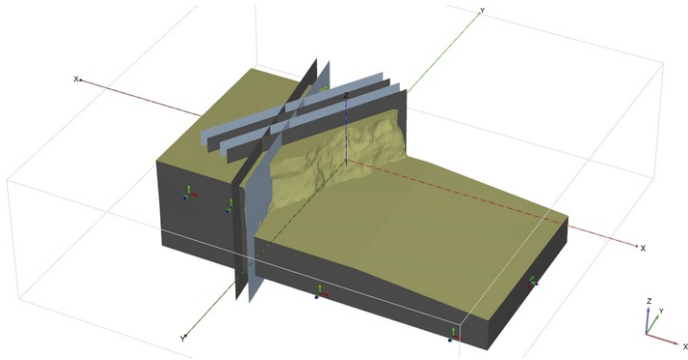


Figure 14. Fig. 14 Three-dimensional solid forming the whole analysis domain and indications of the joint interfaces.

alt-text: Fig. 14

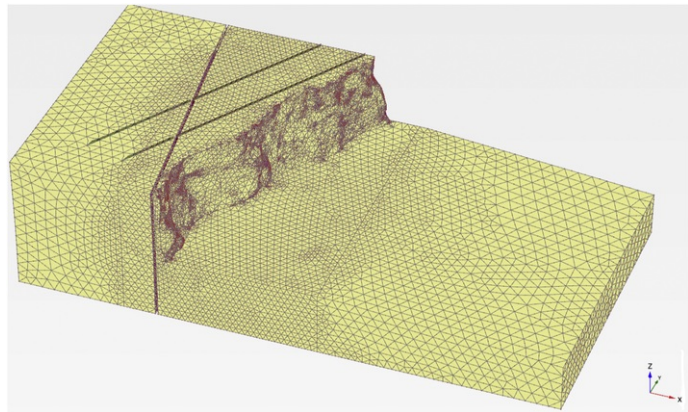


Figure 15. Fig. 15 Three-dimensional finite element discretization mesh.

alt-text: Fig. 15

Table 2. Table 2 Mechanical parameters adopted in the FEM analysis.

alt-text: Table 2

Mechanical Parameters	c_i (kPa)	ϕ_i (°)	σ_t (kPa)
Uncemented interfaces	1	27	1
Slightly cemented interfaces	10	27	10
Intact rock	100	27	120

Under these assumptions, numerical convergence is not reached in all the analyses independently from the intact rock cohesion value assumed and a failure mechanism develops within the domain. In particular, the unstable area is represented by the front portion of the cliff that is delimited at rear by the interfaces introduced. As a matter of fact, both the vertical displacements (Fig. 16) and the horizontal displacements (Fig. 17) appear to be concentrated in this cliff portion delimited by the interfaces. Even with high values of the intact rock cohesion, the cliff becomes unstable, so that a clear role of the uncemented joints in the control of the cliff stability is observed. These results are

not consistent with those obtained by the simulations proposed by Mancini et al. (2017), where continuity conditions are instead supposed for the whole rock mass. Figure 17 shows that the larger horizontal displacements are seen in the lower part of the cliff portion protruding in the sea, characterized by no lateral confinement, whereas Figure 16 indicates that the larger vertical displacements are calculated in the upper part of the same rock portion. The same results are more clearly observed in the vertical cross-section shown in Figures 18 and 19. In fact, both the figures show that the failure mechanism develops from the toe of the cliff according to a steep failure surface and then reaches the existing rear joint, thus connecting with the top of the cliff. This numerical mechanism of rock portion detachment from the cliff is compatible with the collapses that have been observed in the surrounding areas of the cliff.

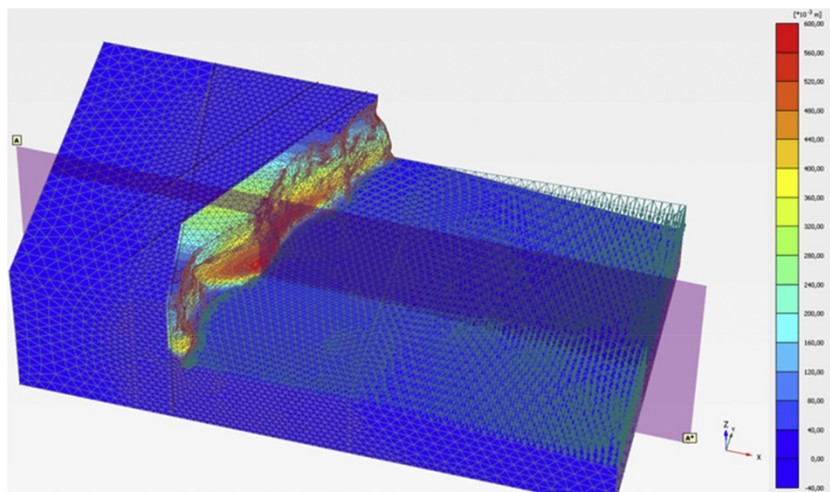


Figure 16, Fig. 16 Horizontal displacements calculated.

alt-text: Fig. 16

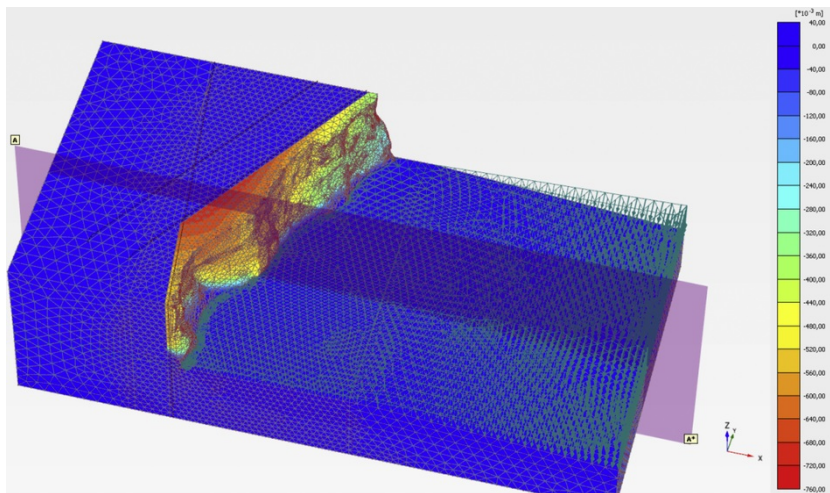


Figure 17, Fig. 17 Vertical displacements calculated.

alt-text: Fig. 17

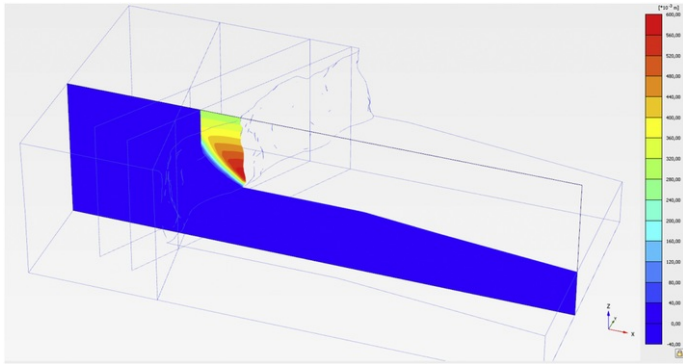


Figure 18, Fig. 18 Horizontal displacements calculated for cross-section A-A*

alt-text: Fig. 18

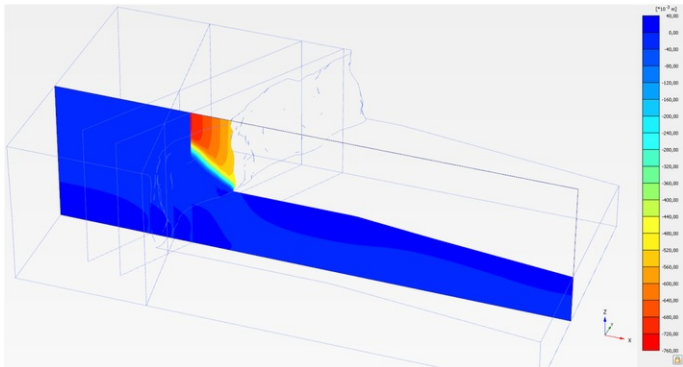


Figure 19, Fig. 19 Vertical displacements calculated for cross-section A-A*

alt-text: Fig. 19

Later on, the case of a slightly cemented rear fracture was considered and the parameters used are indicated in Table 2. In this case, unlike the case of uncemented rear joint, the analyses converge for even low values of intact rock cohesion. Only when very low values of c_0^i are used ($c_0^i = 35$ – 40 kPa) the cliff tends to collapse (Fazio et al., 2017). This result is very similar to the continuous model proposed by Mancini et al. (2017), for which the same limiting cohesion value and the same failure mechanism are simulated. When shear parameters of the rear joint equal to those of the intact rock are used, the numerical results tend to be similar to those of the continuous model.

4.4 CONCLUDING REMARKS

In this paper a comprehensive methodology aimed at assessing hazard conditions related to the stability of sea rocky cliffs was proposed as first and then the corresponding application to a case study was developed. The methodology includes a detailed survey of the cliff geometry by means of UAV-based point cloud, geological and geomechanical surveys of the area, a mapping of the discontinuities of the rock mass based on the UAV survey, to be validated with conventional in-situ geosstructural reliefs, a laboratory testing campaign for defining the geomechanical properties of the rock materials and finally two- and three-dimensional finite element models of the study cliff, which implement the most important discontinuities detected in the rock mass affecting the stability of the sea cliff. An application of the methodology to a soft carbonate rock sea cliff was then carried out and the results were compared with the typical failure processes observed in the study area. In particular, UAV-based mapping was recognized to be successful to detect the most unfavorable discontinuities existing in the rock mass, according to the results of a traditional field geosstructural survey and, as such, this method can be considered to be reliable especially for those situations where the cliff exposed cliff faces are not directly accessible. Limits of applicability was stated for closed/tight discontinuities which were directly recognized and measured by in situ traditional methods but not by the UAV survey. In the specific case, this was observed for all the faults or fractures strike approximately perpendicular to the cliff face.

Detailed laboratory tests were carried out on intact rock samples taken from a nearby quarry in order to determine the physical and mechanical properties, both under wet and dry conditions, of the two geotechnical units present along the cliff. In particular, a strong influence of the saturation conditions of the sample belonging to the two geotechnical units was observed according to the test results, since the UCS and ITS strengths at the saturated state were found less than half of the corresponding value under dry conditions, especially for the calcisiltite unit. In fact, the calcisiltites exhibit less overall strength and more susceptibility to erosion and degradation, both at the meso-scale and the macro-scale, than calcarenites and at places the instability mechanisms are just controlled by the contrast in shear strength and stiffness between the these units.

The two-dimensional finite element model was based on the results of the in situ geostructural and geomechanical surveys, using the weighted mean for the geotechnical parameters of the different units defined on the cliff face. The three-dimensional finite element model was defined in accordance with the detailed cliff surface geometry derived from the UAV-survey and has implemented the most important structural features of the rock mass by means of interface elements. The results of modeling indicate the open vertical discontinuities strike approximately parallel to the cliff face with the most unfavourable orientation from the stability point of view and the combination of this structural condition with erosion and climate-induced rock mechanical weathering can bring the cliff close to failure movements. Moreover, the failure mechanisms obtained by both FEM analysis agree well with those typically observed in the study area. These results confirm the importance of numerical modeling techniques in defining the orientation of the most unfavourable discontinuities affecting the cliff stability and providing a parametric analysis able to give both qualitative and quantitative information on the potential failure mechanisms and the likelihood of the potential failure occurring. At the same time, the importance of detailed in situ surveys by traditional methods, geostructural and geomechanical in types, is evident, both to validate the models obtained by UAV technology and to base FEM analysis on real geometrical data about rock masses consisting of both rock blocks and discontinuities.

Uncited references

[Andriani and Walsh, 2002](#)

[Ciantia et al., 2015](#)

[Pikelj et al., 2018](#)

[PLAXIS, n.d](#)

[PLAXIS, n.d](#)

REFERENCES

Abellan A., Derron M.H. and Jaboyedoff M., Use of 3D Point Clouds in Geohazards, *Remote Sens.* **8**, 2016, 130, <https://doi.org/10.3390/rs8020130>.

Agüera-Vega F., Carvajal-Ramírez F. and Martínez-Carricondo P., Accuracy of digital surface models and orthophotos derived from unmanned aerial vehicle photogrammetry, *J. Surv. Eng.* **143** (2), 2016, , 04016025 [https://doi.org/10.1061/\(ASCE\)SU.1943-5428.0000206](https://doi.org/10.1061/(ASCE)SU.1943-5428.0000206).

Andriani G.F. and Parise M., Applying rock mass classifications to carbonate rocks for engineering purposes with a new approach using the rock engineering system, *Journal of Rock Mechanics and Geotechnical Engineering* *J. Roc Mech. Geotech. Eng.* **9** (2), 2017, 364–369, 6.

Andriani G.F. and Pellegrini V., Qualitative assessment of the cliff instability susceptibility at a given scale with a new multidirectional method, *Int. J. of Geol.* **2014** (8), 2014, 73–80.

Andriani G.F. and Walsh N., Physical properties and textural parameters of calcarenitic rocks: qualitative and quantitative evaluations, *Engineering Geology* *Eng. Geol.* **67** (1–2), 2002, 5–15.

Andriani ~~G.F.~~ and Walsh N., Petrophysical and mechanical properties of soft and porous building rocks used in apulian monuments (South Italy), *Geol. Soc., London, Spec. Publ.* **333**, 2010, 129–141.

Assali P., Grussenmeyer P., Villemin T., Pollet N. and Viguier F., Surveying and modeling of rock discontinuities by terrestrial laser scanning and photogrammetry: Semi-automatic approaches for linear outcrop inspection, *J. Struct. Geol.* **66**, 2014, 102–114, <https://doi.org/10.1016/j.jsg.2014.05.014>.

Balek J. and Blahůt J., A critical evaluation of the use of an inexpensive camera mounted on a recreational unmanned aerial vehicle as a tool for landslide research, *Landslides* **14**, 2017, 1217–1224, <https://doi.org/10.1007/s10346-016-0782-7>.

Bemis S.P., Micklethwaite S., Turner D., James M.R., Akciz S., Thiele S.T. and Bangash H.A., Ground-based and UAV-based photogrammetry: **Aa** multi-scale, high-resolution mapping tool for structural geology and paleoseismology, *J. Struct. Geol.* **69**, 2014, 163–178, <https://doi.org/10.1016/j.jsg.2014.10.007>.

- Brideau M.A., Pedrazzini A., Stead D., Froese C., Jaboyedoff M. and van Zeyl D., Three-dimensional slope stability analysis of South Peak, Crowsnest Pass, Alberta, Canada, *Landslides* **8**, 2011, 139-158.
- Brideau M.A., Sturenegger M., Stead D., Jaboyedoff M., Lawrence M., Roberts N., Ward B., Millard T. and Clague J., Stability analysis of the 2007 Chehalis lake landslide and airborne LiDAR data, *Landslides* **9**, 2012, 75-91.
- Bryson M., Johnson-Roberson M., Murphy R.J. and Bongiorno D., Kite aerial photography for low-cost, ultra-high spatial resolution multi-spectral mapping of intertidal landscapes, *PLoS One* **8**, 2013, , e73550 <https://doi.org/10.1371/journal.pone.0073550>.
- Buonamici F., Carfagni M., Furferi R., Governi L., Lapini A. and Volpe Y., Reverse engineering modeling methods and tools: a survey, *Computer-Aided Design and Applications* **15** (3), 2018, 443-464.
- Cai M., Practical estimates of tensile strength and Hoek-Brown strength parameter m_i of brittle rocks, *Rock Mech. Rock Eng. Rock Mech. Rock. Eng.* **43** (2), 2010, 167-184.
- Cawood A.J., Bond C.E., Howell J.A., Butler [R.W.R.W.](#) and Totake Y., LiDAR, UAV or compass-clinometer? Accuracy, coverage and the effects on structural models, *J. Struct. Geol.* **98**, 2017, 67-82, <https://doi.org/10.1016/j.jsg.2017.04.004>.
- Ciantia [M.-O.M.O.](#), Castellanza R. and Di Prisco C., Experimental study on the water-induced weakening of calcarenites, *Rock Mech. Rock Eng. Rock Mech. Rock. Eng.* **48** (2), 2015, 441-461.
- Corsini A., Castagnetti C., Bertacchini E., Rivola R., Ronchetti F. and Capra A., Integrating airborne and multi-temporal long-range terrestrial laser scanning with total station measurements for mapping and monitoring a compound slow moving rock slide, *Earth Surf. Proc. Landf.* **38**, 2013, 1330-1338, <https://doi.org/10.1002/esp.3445>.
- Cracknell [M.-J.M.I.](#), Roach M., Green D. and Lucieer A., Estimating bedding orientation from high-resolution digital elevation models, *IEEE Transactions on Geoscience and Remote Sensing* *IEEE Trans. Geosci. Remote Sens.* **51** (5), 2013, 2949-2959.
- Del Gaudio V., Pierri P., Frepoli A., Calcagnile G., Venisti N. and Cimini G., A critical revision of the seismicity of Northern Apulia (Adriatic Microplate - Southern Italy) and implications for the identification of seismogenic structures, *Tectonophysics* **436** (1/4), 2007, 9-35. [\(Please add after this reference the reference: Fazio, N.L., Perrotti, M., Lollino, P., Parise, M., Vattano, M., Madonia, G., Di Maggio, C., 2017. A three-dimensional back-analysis of the collapse of an underground cavity in soft rocks. Eng. Geol. 228 \(13\), 301-311.\)](#)
- Ferrero A.M., Migliazza M., Roncella R. and Rabbi E., Rock slopes risk assessment based on advanced geostructural survey techniques, *Landslides* **8**, 2011, 221-231, <https://doi.org/10.1007/s10346-010-0246-4>.
- Fonstad M.A., Dietrich J.T., Courville B.C., Jensen [J.H.L.](#) and Carbonneau P.E., Topographic structure from motion: [Aa](#) new development in photogrammetric measurement, *Earth Surf. Process. Landf.* **38**, 2013, 421-430, <https://doi.org/10.1002/esp.3366>.
- Genchi S.A., Vitale A.J., Perillo G.M. and Delrieux C.A., Structure-from-motion approach for characterization of bioerosion patterns using UAV imagery, *Sensors* **15**, 2015, 3593-3609, <https://doi.org/10.3390/s150203593>.
- Giordan D., Manconi A., Facello A., Baldo M., Dell'Anese F., Allasia P. and Dutto F., Brief Communication: [Ft](#)he use of an unmanned aerial vehicle in a rockfall emergency scenario, *Nat. Hazards Earth Syst. Sci.* **15**, 2015, 163-169, <https://doi.org/10.5194/nhess-15-163-2015>.
- Hirschmuller [H.H.](#), Stereo processing by semiglobal matching and mutual information, *IEEE T. on Pattern Anal.* **30** (2), 2008, 328-341, <https://doi.org/10.1109/TPAMI.2007.1166>.
- Hoek E. and Brown E.T., Empirical strength criterion for rock masses, *J. Geotech Engng. Div., ASCE* **106** (GT 9), 1980, 1013-1035.
- Hoek E., Carranza-Torres C. and Corkum B., Hoek-Brown failure criterion, In: *Proceedings of the NARMS-TAC Conference*, 2002, 267-273, (Toronto).
- ISRM, Suggested methods for determining the uniaxial compressive strength and deformability of rock materials, *Int. J. Rock Mech. Min. Sci. Int. J. Rock Mech. Min. Sci.* **16** (2), 1979, 135-140.
- ISRM, In: Brown E., (Ed), *Rock Characterization Testing and Monitoring*, 1981, Pergamon Press; Oxford.
- ISRM, Suggested Methods for the Quantitative Description of Discontinuities in Rock Masses, *International Journal of Rock Mechanics and Mining Sciences & Geomechanics Abstracts* **15**, 1978, 319-368.
- James M.R. and Robson S., Straightforward reconstruction of 3D surfaces and topography with a camera: Accuracy and geoscience application, *J. Geophys. Res. Earth* **117**, 2012, <https://doi.org/10.1029/2011JF002289>.
- Lollino P. and Andriani G.F., Role of Brittle Behaviour of Soft Calcarenites [Uu](#)nder Low Confinement: Laboratory Observations and Numerical Investigation, *Rock Mechanics and Rock Engineering* *Rock Mech. Rock. Eng.* **50** (7),

2017, 1863-1882.

Lowe D.G., Distinctive image features from scale invariant keypoints, *Int. J. Comput. Vision**Int. J. Comput. Vis.* **60** (2), 2004, 91-110, <https://doi.org/10.1023/B:VISI.0000029664.99615.94>.

Mancini F., Dubbini M., Gattelli M., Stecchi F., Fabbri S. and Gabbianelli G., Using unmanned aerial vehicles (UAV) for high-resolution reconstruction of topography: The structure from motion approach on coastal environments, *Remote Sens.* **5**, 2013, 6880-6898, <https://doi.org/10.3390/rs5126880>.

Mancini F., Castagnetti C., Rossi P., Dubbini M., Fazio N.L.N.L., Perrotti M. and Lollino P., An Integrated Procedure to Assess the Stability of Coastal Rocky Cliffs: From UAV Close-Range Photogrammetry to Geomechanical Finite Element Modeling, *Remote Sensing**Remote Sens.* **9** (12), 2017, 1235.

Marinos P. and Hoek E., Estimating the geotechnical properties of heterogeneous rock masses such as flysch, *Bull Eng Geol Env* **60**, 2001, 82-92.

Martino S. and Mazzanti P., Integrating geomechanical surveys and remote sensing for sea cliff slope stability analysis: the Mt. Pucci case study (Italy), *Nat. Hazards Earth Syst. Sci.* **14**, 2014, 831-848.

Michoud C., Carrea D., Costa S., Derron M.H., Jaboyedoff M., Delacourt C., Maquaire O., Letortu P. and Davidson R., Landslide detection and monitoring capability of boat-based mobile laser scanning along Dieppe coastal cliffs, Normandy, *Landslides* **12**, 2015, 403-418, <https://doi.org/10.1007/s10346-014-0542-5>.

Nex F. and Remondino F., UAV for 3D mapping applications: a review, *Appl. Geomat.* **6**, 2014, 1-15, <https://doi.org/10.1007/s12518-013-0120-x>.

Pikelj K., Ružić I., Ilić S., James M., R. Y. and Kordić B., Implementing an efficient beach erosion monitoring system for coastal management in Croatia, *Ocean and Coastal Management**Ocean Coast. Manag.* **156**, 2018, 223-238, <https://doi.org/10.1016/j.ocecoaman.2017.11.019>.

Piras M., Taddia G., Forno M.G., Gattiglio M., Aicardi I., Dabove P., Lo Russo S. and Lingua A., Detailed geological mapping in mountain areas using an unmanned aerial vehicle: application to the Rodoretto Valley, NW Italian Alps, *Geomat. Nat. Hazards Risk* **8**, 2017, 137-149, <https://doi.org/10.1080/19475705.2016.1225228>.

[PLAXIS 2D \[Computer software\]](#)[PLAXIS-BV, 2018](#). Plaxis-[2D Reference Manual](#), Delft, Netherlands.

[PLAXIS 3D \[Computer software\]](#)[PLAXIS-BV, 2013](#). Plaxis-[3D Reference Manual](#), Delft, Netherlands.

Quinn J.D., Rosser N.J., Murphy W. and Lawrence J.A., Identifying the behavioural characteristics of clay cliffs using intensive monitoring and geotechnical numerical modelling, *Geomorphology* **120**, 2010, 107-122, <https://doi.org/10.1016/j.geomorph.2010.03.004>.

Riquelme A.J., Tomás R. and Abellán A., Characterization of rock slopes through slope mass rating using 3D point clouds, *Int. J. Rock Mech. Min. Sci.* **84**, 2016, 165-176, <https://doi.org/10.1016/j.ijrmms.2015.12.008>.

Romana M., New adjustment ratings for application of Bieniawski classification to slopes, In: *Proceedings of the International Symposium on the Role of Rock Mechanics in Excavations for Mining and Civil Works. International Society of Rock Mechanics*, 1985, 49-53, (Zacatecas).

Rossi P., Mancini F., Dubbini M., Mazzone F. and Capra A., Combining nadir and oblique UAV imagery to reconstruct quarry topography: methodology and feasibility analysis, *Eur. J. Remote Sens.* **50** (1), 2017, 211-221, <https://doi.org/10.1080/22797254.2017.1313097>.

Rupnik E., Nex F. and Remondino F.E., Oblique multi-camera systems-orientation and dense matching issues, In: *EuroCOW 2014, Proceedings of the European Calibration and Orientation Workshop, Castelldefels, Spain, 12-14 February 2014*, **Volume XL-3/W1**, 2014, The International Archives of Photogrammetry, Remote Sensing and Spatial Information Sciences: 2014, 107-114, <https://doi.org/10.5194/isprsarchives-XL-3-W1-107-2014>.

Rutzinger M., Maukisch M., Petrini-Monteferrri F. and Stötter J., Development of algorithms for the extraction of linear patterns (lineaments) from airborne laser scanning data, In: *Proceedings of the Conference 'Geomorphology for the Future'*, 2007, Obergurgl.

Ružić I., Marović I., Benac Č., et al., Coastal cliff geometry derived from Structure-from-Motion photogrammetry at Stara Baška, Krk Island, Croatia, *Geo-Mar Lett**Geo-Mar. Lett.* **34**, 2014, 555, <https://doi.org/10.1007/s00367-014-0380-4>.

Schumaker L.L., Triangulations in CAGD, *IEEE Comput. Graph.* **13** (1), 1993, 47-52.

Snaveley N., Seitz S.M. and Szeliski R., Photo tourism: Exploring photo collections in 3D, *ACM Transactions on Graphics* *ACM Trans. Graph.* **25** (3), 2006, 835-846, <https://doi.org/10.1145/1141911>.

Warrick J.A., Ritchie A.C., Adelman G., Adelman K. and Limber P.W., New techniques to measure cliff change from historical oblique aerial photographs and Structure-from-Motion photogrammetry, *J. Coast. Res.* **33**, 2016, 39-55, <https://doi.org/10.2112/JCOASTRES-D-16-00095.1>.

Westoby M.J., Brasington J., Glasser N.F., Hambrey M.J. and Reynolds J.M., 'Structure-from-Motion' photogrammetry: A low-cost, effective tool for geoscience applications, *Geomorphology* **179**, 2012, 300-314, <https://doi.org/10.1016/j.geomorph.2012.08.021>.

Highlights

- Detailed three-dimensional geometrical survey of the cliff by means of UAV-based photogrammetry techniques;
- Detection of the most relevant fractures and joint sets by means of the analysis of UAV models;
- Geological, geostructural and geomorphological analysis of the cliff by means of in-situ surveys;
- Mechanisms obtained by FEM analysis agree well with those typically observed in the study area;
- **Results confirm the importance of numerical modeling techniques in defining the orientation of the most unfavourable discontinuities affecting the cliff stability.**

Queries and Answers

Query:

Your article is registered as a regular item and is being processed for inclusion in a regular issue of the journal. If this is NOT correct and your article belongs to a Special Issue/Collection please contact d.perumal@elsevier.com immediately prior to returning your corrections.

Answer: Yes

Query:

Please confirm that given names and surnames have been identified correctly and are presented in the desired order, and please carefully verify the spelling of all authors' names.

Answer: Yes

Query:

The author names have been tagged as given names and surnames (surnames are highlighted in teal color). Please confirm if they have been identified correctly.

Answer: Yes

Query:

Highlights should only consist of 125 characters per bullet point, including spaces. The highlights provided are too long; please edit them to meet the requirement.

Answer: ok

Query:

The citation "Romana, 1985" has been changed to "Romana, 1985" to match the author name/date in the reference list. Please check if the change is fine in this occurrence and modify the subsequent

occurrences, if necessary.

Answer: the change is fine.

Query:

The citation "Romana 1995" has been changed to "Romana, 1985" to match the author name/date in the reference list. Please check if the change is fine in this occurrence and modify the subsequent occurrences, if necessary.

Answer: the change is fine.

Query:

Please note that Fig. 12 was not cited in the text. Please check if the suggested citation is appropriate, and correct if necessary.

Answer: The suggested citation It's not appropriate. Please see Comments below.

Query:

Citation "PlaxisBV, 2017" has not been found in the reference list. Please supply full details for this reference.

Answer: all the citation has been correct

Query:

Uncited references: This section comprises references that occur in the reference list but not in the body of the text. Please position each reference in the text or, alternatively, delete it. Thank you.

Answer: Pikelj et al is now correct; Andriani and walsh, 2002, Plaxis citations and ciantia et al 2015 are now correct.

Query:

Correctly acknowledging the primary funders and grant IDs of your research is important to ensure compliance with funder policies. We could not find any acknowledgement of funding sources in your text. Is this correct?

Answer: This research work was supported by Regione Puglia - Civil Protection Department, in the framework of the project "Integrated assessment of geo-hydrological instability phenomena in the Apulia region, interpretative models and definition of rainfall thresholds for landslide triggering" funded by P.O.R. Puglia 2014-2020, Asse V - Azione 5.1. - B82F16003840006. It was also supported by the framework of the project Interreg III A- "WET SYS B" 2000-2006, with the financial contribution by the European Community.